Atmos. Chem. Phys. Discuss., 13, 18905–18950, 2013
www.atmos-chem-phys-discuss.net/13/18905/2013/
doi:10.5194/acpd-13-18905-2013

Atmospheric Chemistry and Physics
Discussions
Open Access

Interaction between dynamics and thermodynamics during tropical cyclogenesis

S. Gjorgjievska and D. J. Raymond

Physics Department and Geophysical Research Center, New Mexico Institute of Mining and Technology, Socorro, New Mexico 87801, USA

Received: 26 April 2013 – Accepted: 3 July 2013 – Published: 16 July 2013

Correspondence to: S. Gjorgjievska (saska@nmt.edu)

Published by Copernicus Publications on behalf of the European Geosciences Union.

Abstract

Observational data of tropical disturbances are analyzed in order to investigate tropical cyclogenesis. Data from 31 cases observed during two field campaigns are used to investigate possible correlations between various dynamic and thermodynamic variables. The results show that a strong mid-level vortex is necessary to promote spin up of the low-level vortex in a tropical cyclone. This paper presents a theory on the mechanism of this process; the mid-level vortex creates a thermodynamic environment conducive to convection with a more bottom-heavy mass flux profile that exhibits a strong positive vertical gradient in a shallow layer near the surface. Mass continuity then implies that the strongest horizontal mass and vorticity convergence occur near the surface. This results in low-level vortex intensification.

For two of the disturbances that were observed during several consecutive days, evolution of the dynamics and thermodynamics is documented. One of these disturbances, Karl, was observed in the period before it intensified into a tropical storm; the other one, Gaston, was observed after it unexpectedly decayed from a tropical storm to a tropical disturbance. A hypothesis on its decay is presented.

1 Introduction

The genesis phase is the least understood part of the tropical cyclone life cycle. In this paper we use the term cyclogenesis to refer to the intensification of a precursor disturbance into a tropical storm (TS). We know that tropical storms develop from preexisting finite amplitude disturbances, such as mesoscale convective systems (MCS) that exhibit cyclonic vertical vorticity. They often form within monsoon troughs or tropical waves. Genesis involves processes that are much less important during the mature phase of a tropical cyclone. Favorable conditions for these MCSs to develop into tropical storms are high sea surface temperature and low vertical wind shear. These conditions are probably the best summarized by Gray (1968). However, although

ACPD

13, 18905–18950, 2013

Title Page
Abstract | Introduction
Conclusions | References
Tables | Figures
◀| |▶
◀ ▶
Back | Close
Full Screen / Esc
Printer-friendly Version
Interactive Discussion

during a hurricane season many MCSs develop, only small percentage of these turn into tropical storms, even in favorable environmental conditions. How are the developing disturbances different than the non-developing? McBride and Zehr (1981) compared composites of non-developing and developing cloud clusters. Their main findings were: both systems have warm cores in the upper levels, but the warming is more pronounced in the developing clusters; the static stability is somewhat smaller for the developing systems; the developing composites exhibit less vertical wind shear near the system center, but there is a requirement for certain kind of wind shear surrounding the developing system; and the developing clusters exhibit larger positive vorticity at low levels. Perhaps more detailed observations of the evolution of both developing and non-developing disturbances would help to quantify better the differences and this will hopefully help our understanding of the mechanisms of tropical cyclogenesis.

Today there exist two types of hypotheses of tropical cyclogenesis. Dunkerton et al. (2009) hypothesized that genesis is initiated within westward moving tropical waves, in a region near the intersection of the wave axis and the critical latitude. The latter is defined as the latitude at which the wave speed is as same as the background flow. They call this intersection a sweet spot, and the broader recirculating area around it is dubbed the pouch. The pouch exhibits low-level cyclonic vorticity and minimal strain rate. The air within the pouch is protected from lateral dry air intrusion, and thus continuous moist convection is enabled, which further increases the cyclonic vorticity. Ultimately, the wave-convection interaction leads to development of rotating deep convection. Aggregation of low-level vorticity associated with the rotating deep convection results in a vortex intensification in the lower troposphere, and subsequently in the middle and upper troposphere. The vortex eventually separates from the mother wave. This hypothesis represents so-called "bottom-up" development.

The other type of hypothesis postulates a "top-down" development. In this case a mid-level vortex develops first. In thermal wind balance, this situation corresponds to a cold-core vortex below the vorticity maximum and a warm core vortex aloft. Later the near-surface vorticity increases and subsequently a warm-core vortex develops

ACPD
13, 18905–18950, 2013

in the lower troposphere and genesis occurs. There exists observational evidence for this pathway of development (Harr and Elsberry, 1996; Bister and Emanuel, 1997; Raymond et al., 1998; Raymond and Lopez, 2011; Davis and Ahijevych, 2012, and others). Nolan (2007) used a model to simulate development of tropical cyclones, initiating each simulation with a preexisting vortex. All of his simulations, even the ones initiated with a low-level vortex, first developed a mid-level vortex before intensification of the low-level vortex occurred. The question that arises here is how the mid-level vortex encourages vorticity intensification near the surface. Bister and Emanuel (1997) and others have hypothesized that the mid-level vortex extends downwards in conditions of stratiform rain, after which a warm core develops. The process of this downward vortex extension, however, is not explained. Raymond et al. (2011), hereafter RSL11, suggest that the thermodynamic state of the atmosphere within the mid-level vortex favors convection that aids the formation of the low-level vortex.

In the present paper we analyze data from developing and non-developing disturbances that were observed during the 2010 hurricane season in the Tropical Atlantic and the Caribbean. For part of the analysis we also use data gathered in the West Pacific during the 2008 typhoon season. The results support the establishment of a mid-level vortex preceding genesis.

There are two purposes of this paper. First, it proposes a theory on tropical storm formation, which we call the hybrid hypothesis. Second, it presents a hypothesis of how an observed storm decayed. The remainder of this paper is organized as follows. The second section of this paper describes the data and the methods that are used to analyze the data. Section 3 gives the equations we use for our calculations, and the results from our analysis are presented in Sect. 4. We discuss the results and attempt to explain the mechanisms of hybrid cyclogenesis in Sect. 5.

ACPD
13, 18905–18950, 2013

S. Gjorgjievska and D. J. Raymond

2 Data and methods

Two data sets are used for the purpose of our analysis. One set was gathered during the field campaign Pre-Depression Investigation of Cloud systems in the Tropics (PREDICT). The objectives and the tools of this campaign are described by Montgomery et al. (2012). The target areas of research were the North Atlantic and the Caribbean. The campaign took place during the period August–September of 2010 and was based on the island of St. Croix in the Caribbean. The main tools for gathering data were dropsondes. About twenty-five dropsondes per mission were launched from the National Science Foundation (NSF)-National Center for Atmospheric Research (NCAR) research aircraft, Gulfstream V (G-V). The aircraft was also equipped with on-board instrumentation for measuring different meteorological parameters, but for our analyses we use the dropsonde data only. The launching altitude was 11–13 km, so that data were recorded throughout almost the entire depth of the troposphere. Roughly, the dropsondes were distributed on a rectangular longitude-latitude grid, with grid spacing approximately 1°. The data were quality controlled and processed by NCAR's Earth Observing Laboratory (EOL). Twenty-six missions were conducted during which approximately 600 dropsondes were released. Eight disturbances were observed, for most of which multiple missions were flown. Four of these intensified into tropical storms, one of which became a category 3 hurricane.

The other data set was gathered during the field campaign Tropical Cyclone Structure (TCS08) experiment that took place in the period August–September 2008. The Naval Research Laboratory (NRL) P-3 aircraft and two Air Force Reserve WC-130 aircraft deployed dropsondes over the West Pacific. In addition, the P-3 aircraft made wind measurements using the ELDORA radar. The quality control on the dropsonde data was also done by EOL. See Raymond and Lopez (2011) for more information.

Dropsondes measure temperature, pressure, horizontal wind and relative humidity continuously as they descend, so that the vertical resolution of the collected data is good. However, the horizontal resolution is coarse ($\sim 1^\circ \times 1^\circ$). We further use a three

ACPD
13, 18905–18950, 2013

dimensional variational (3-D-Var) analysis, to obtain values of the meteorological parameters in the entire observational volume. For each mission we first vertically interpolate the data from each dropsonde, so that they all have the same vertical interval and step size. We then also calculate the mixing ratio, moist entropy, saturation mixing ratio, and saturation moist entropy at every grid point. The dropsondes are not launched at the same time but rather one at a time, roughly one dropsonde every 7–10 min. Depending on the size of the disturbance, it takes about 2–4 h for all the dropsondes to be released. For the purpose of our analyses we adjust dropsonde positions in the moving frame of the disturbance to their locations at a standard reference time. The moving frame is defined as a frame moving with the propagation velocity of the disturbance. The propagation velocity is calculated from the Final Analysis (FNL) for the Global Forecasting System by tracking the vorticity center averaged between 850–700 hPa. The standard reference time is usually chosen to be roughly half way through the period of dropsonde deployment, resulting in a snapshot of the disturbance at this time. The snapshot assumption is adequate for studying mesoscale processes. Then we specify a three dimensional grid, moving with the observed disturbance, with longitude–latitude resolution $0.125^\circ \times 0.125^\circ$, and vertical resolution of 0.625 km. The dropsonde data are assigned to appropriate grid points. The data are then interpolated to the full grid using the 3-D-Var scheme. The vertical velocity is calculated by strongly enforcing mass continuity in the 3-D-Var scheme. The 3-D-Var analysis also imposes a certain degree of smoothing in order to remove noise and aliasing. Finally, we mask the file in order to consider only the area covered by the dropsondes. The 3-D file at this point is ready for analysis.

A detailed description of the 3-D-Var technique used in the present work is given by Lopez and Raymond (2011) and Raymond and Lopez (2011). The values of the 3-D-Var parameters used here are the same as in RSL11.

3 Equations

3.1 Vorticity budget equation

We adopt the flux form of the vorticity budget equation from Raymond and López (2011):

$$\frac{\partial \zeta_z}{\partial t} = -\nabla_h \cdot (\zeta_z \boldsymbol{v}_h - \boldsymbol{\zeta}_h v_z + \widehat{k} \times \boldsymbol{F}) - \widehat{k} \cdot \nabla_h \theta \times \nabla_h \Pi. \tag{1}$$

Here, $\boldsymbol{v} = (\boldsymbol{v}_h, v_z)$ is the storm-relative velocity, $\boldsymbol{\zeta} = (\boldsymbol{\zeta}_h, \zeta_z)$ is the absolute vorticity, $\boldsymbol{F}$ is a force due to surface friction, θ is the potential temperature, and $\widehat{k}$ is the unit vector in the vertical direction. The quantity $\Pi = C_P (p/p_{\mathrm{ref}})^{R/C_P}$ is the Exner function, where C_P is the specific heat at constant pressure, R is the gas constant for dry air and $p_{\mathrm{ref}} = 1000\,\mathrm{hPa}$ is a constant reference pressure. The subscripts h and z denote the horizontal and vertical components, respectively. The last term on the right hand side represents the vertical component of the baroclinic generation of vorticity. For environments that are characterized by weak baroclinicity, as in the tropics, this term is insignificant and thus can be neglected. The expression in parentheses is the horizontal flux of ζ_z: the first term represents the flux due to advection, the second is the flux due to tilting, and the third is the flux due to the frictional force. The frictional force per unit mass, $\boldsymbol{F}$, is estimated by

$$\boldsymbol{F} = \boldsymbol{\tau} \frac{\exp(-z/z_{\mathrm{s}})}{\rho z_{\mathrm{s}}}, \tag{2}$$

where z is the height, z_{s} is a scale height which represents the average depth of the boundary layer, and

$$\boldsymbol{\tau} = -\rho_{\mathrm{bl}} C_{\mathrm{D}} |\boldsymbol{U}_{\mathrm{bl}}| \boldsymbol{U}_{\mathrm{bl}} \tag{3}$$

ACPD
13, 18905–18950, 2013
Interaction between dynamics and thermodynamics
S. Gjorgjievska and D. J. Raymond

is the surface stress. The symbol ρ represents the density, and $\boldsymbol{U}$ is the horizontal wind in the reference frame of the Earth. The subscript bl stands for boundary layer and C_D is a drag coefficient, which we calculate using the bulk formula

$$C_D = (1 + 0.028|\boldsymbol{U}_{bl}|) \times 10^{-3}. \quad (4)$$

Here $\boldsymbol{U}_{bl}$ has units of meters per second. This is the same formula for the drag coefficient as used in RSL11.

3.1.1 Thermodynamic variables

Two important parameters that we analyze are the saturation fraction and the instability index. The saturation fraction is defined as the vertically integrated precipitable water divided by the vertically integrated saturated precipitable water,

$$\mathrm{SF} = \frac{\int_0^h \rho r \mathrm{d}z}{\int_0^h \rho r^* \mathrm{d}z}, \quad (5)$$

where r^* is the saturated mixing ratio. h is the height of the domain. Bretherton et al. (2004) found that this parameter controls most of the variability in rainfall over the tropical oceans. The instability index is a measure of the tropospheric instability to moist convection and it is defined as

$$\Delta s^* = s^*_{\mathrm{low}} - s^*_{\mathrm{high}}. \quad (6)$$

Here s^*_{low} is the saturated moist entropy averaged over the layer between 1 and 3 km and s^*_{high} is the saturated moist entropy averaged over the layer between 5 and 7 km. As the saturated moist entropy is a proxy for temperature at a fixed pressure level, larger values of this parameter are associated with an atmosphere more unstable to moist convection.

ACPD
13, 18905–18950, 2013

S. Gjorgjievska and D. J. Raymond

4 Results

Table 1 shows the date, propagation velocity, reference time, area-averaged Reynolds SST, and National Hurricane Center (NHC) classification for each mission conducted into these disturbances. The results are divided into two parts. The first part presents the more detailed analysis of two disturbances that were observed during PREDICT. One of those, Gaston, had a tropical storm status for a few hours only, after which it started to decay. Nevertheless, it was observed over the course of the next 5 days, as it was expected to intensify again. However, it kept decaying slowly until it dissipated and we take it as a decaying/non-developing case. The other is Karl, a developer that eventually became a major hurricane, that was observed initially in its pre-storm phase. The second part of this section explores possible correlations between dynamic and thermodynamic variables. More precisely, we employ data sets from PREDICT and TCS08 to create scatter plots between these variables, using all available case studies.

Many of the results shown in this paper are obtained by horizontal averaging over an area for each disturbance. A valid question arises here, regarding the proper area to be considered for analysis. Unfortunately, there there does not yet exist an established, objective method for quantitatively comparing the observed disturbances. It is difficult to find such a method, because of inconsistencies among disturbances. There are two main factors driving these inconsistencies. First, there are differences in aircraft data sampling. The observational areas are different sizes and shapes, and the circulation centers are in different locations within the observational area. The other source, which is probably more important but is often neglected, is the uniqueness of each disturbance, regardless of the data sampling area. No two disturbances have the same size, shape, and structure, nor do they occur within identical environments. The pre-storm disturbances in particular are highly non-axisymmetric. Therefore, whatever method is chosen to select an area for analysis will skew the results in some way. For example, one may choose a circular or a rectangular area centered on a circulation center at a certain level for all the disturbances. This area size, for some disturbances may cover

ACPD
13, 18905–18950, 2013

S. Gjorgjievska and D. J. Raymond

50 % of the actual disturbance size, and for some may cover the entire disturbance. Furthermore, in the case of a tilted vortex axis, the results will be skewed in favor of the level for which the circulation center is defined to be the center of the analysis domain. Thus, either choosing the same area, size, and shape for all the disturbances, or subjectively choosing each area for analysis, based on moisture, convective mass flux, and rotation parameters, can each skew the results to some degree.

Keeping the above in mind, we obtained two sets of results. For the first set, averaging was done over a subjectively chosen area for analysis. The criteria were to cover as much of the disturbance as possible, encompass all the convective activity and the high saturation fraction regions; center the area on the 5 km circulation center if possible, without significantly compromising the previous two criteria. For the second set, the analysis was repeated by averaging over the entire observational area, minus the area that was obviously not part of the disturbance. The conclusions of this paper are invariant to the differences between these two sets of results.

To avoid confusion, here we clarify the terminology used throughout the paper. The term mid-level vortex refers to a vortex located anywhere between 3 and 6 km and the significance of this vortex is its association with a cold-core vortex beneath it and a warm-core above it. In other words, there is positive vertical gradient of relative vorticity in a deep layer adjacent to the surface. Whether the maximum vorticity occurs at 4, 5, or 6 km does not affect the interpretation of our findings. With the term lower levels we usually refer to the levels below 3 km, adjacent to the surface, and the term upper levels refers to levels above 5 km.

4.1 Storm analysis

For each disturbance we analyze the evolution of the vertical profiles of vorticity tendency, vertical vorticity, vertical mass flux, moist entropy and saturated moist entropy. The latter is a proxy for the temperature. The vertical profiles of the analyzed variables represent horizontal averages over the respective areas selected for analysis.

ACPD
13, 18905–18950, 2013

4.1.1 Gaston

This disturbance emerged from Africa as an MCS embedded in an easterly wave. Five missions were conducted in this disturbance over the course of 6 days. When the NHC upgraded it from an area of interest to a tropical storm, its location was approximately 36° W, 13° N and it was moving slowly to the WNW. On its first mission in this storm the G-V reached Gaston as it was being downgraded to a tropical depression. Shortly afterward it was further downgraded to an area of interest. The strongest earth-relative wind that the dropsondes registered during Gaston 1 was 13 $\mathrm{m\,s^{-1}}$ near the surface and 16.5 $\mathrm{m\,s^{-1}}$ at 4 km altitude. Figure 1 shows the vertical profiles of area-averaged relative vorticity, vertical mass flux and vorticity tendency. Figure 2 shows area-averaged saturated moist entropy and relative humidity. The red lines correspond to Gaston 1. The relative vorticity at this time had a maximum at 4–5 km, which by the virtue of thermal wind balance implies a cold core below this level and a warm core aloft. Convection occurred in a small region near the 5 km circulation center (see Fig. 10a) and it was surrounded by downdrafts. This explains the small, area-averaged vertical mass flux magnitude (Fig. 1b).

Gaston 2 was conducted the following day. The reference time was close to that of Gaston 1. The green lines in Figs. 1 and 2 show the area averaged vertical structure of Gaston 2. The most obvious feature is that the relative vorticity changed drastically from the previous day. The mid-level vorticity was weaker, even though the vortex was still evident (Fig. 8b). The low-level vorticity, however, was greater, in spite of the negative vorticity tendency from the previous day. This disagreement is most likely due to the fact that the vorticity tendency equation only provides a snapshot at a particular time. The saturated moist entropy remained almost the same in the upper levels, but it exhibited elevated values in the lower levels, in the layer between 0.5 and 3 km (Fig. 2a). As the saturated moist entropy is a proxy for temperature, its increase indicates warming in this layer which by the virtue of the thermal wind balance is in accordance with the weakened mid-level vortex. The vertical mass flux profile at this time exhibited

Discussion Paper | Discussion Paper | Discussion Paper | Discussion Paper |
ACPD
13, 18905–18950, 2013
Interaction between dynamics and thermodynamics
S. Gjorgjievska and D. J. Raymond

maximum near 4 km, but the convective regions covered a smaller fractional area of the disturbance than the downdrafts, so that the magnitude of area-averaged vertical mass flux had not changed from the previous day. The area-averaged relative humidity remained almost the same.

Gaston 3 and Gaston 4 showed a trend (blue and purple lines, respectively, in Figs. 1 and 2) of gradual decrease in the relative vorticity at all levels. Gaston 4 did not exhibit a mid-level circulation center. The relative humidity was decreasing at all levels, especially in the layer between 3 and 8 km. The saturated moist entropy profile implied warming in the lower levels and cooling in the upper levels. In other words, the troposphere was moving towards more unstable stratification. The last mission revealed somewhat increased relative humidity and further warming of the low levels (Figs. 1 and 2, black lines), but this was probably because the disturbance had moved over the warmer Caribbean waters. Smith and Montgomery (2012) also found that as Gaston was decaying, CAPE was increasing, which is in agreement with our findings.

We hypothesize that the severe decrease of the mid-level vortex in the period between the first two missions was a deciding factor for Gaston's failure to re-intensify. The rationale behind this is discussed in Sect. 5.

4.1.2 Karl

Karl started as a disturbance within the ITCZ, just northeast of the South American coast. It was a broad low pressure area with active convection. G-V conducted six missions total into this disturbance, the first two of which took place well before the NHC declared it to be an area of interest. Thus, the genesis phase of Karl, which ultimately developed into a category 3 hurricane, was well captured.

Because of air space restrictions, the fourth research flight did not cover an adequate observational area (the circulation center was not even partly covered) and therefore we disregard the analysis from that mission. The results from the other 5 missions are summarized in Figs. 3 and 4. Karl 1 was conducted on 10 September. The disturbance had obvious vorticity at low levels as well as at mid-levels with a SW tilt of the vorticity

ACPD
13, 18905–18950, 2013

axis (not shown). The relative vorticity was largest in the lowest kilometer as the red line in Fig. 3a shows, but nevertheless it was small overall and the wind speed near the surface did not exceed $12\,\mathrm{m\,s^{-1}}$ in the earth-relative frame. The mass flux profile reflects the large convective activity that was occurring at that time. The convective flux was bottom heavy, which suggests that extensive stratiform regions did not exist at that time. The entire column was moist, as Fig. 4b shows, for an area-averaged saturation fraction of 0.79. The vorticity tendency was overall positive, though small in magnitude (Fig. 3c). Several hours later the Karl 2 mission was conducted (the reference times of the two missions were about 9 h apart). The most notable change was in the mass flux profile which was now top heavy (Fig. 3b, green line), suggesting dominance of stratiform clouds, which perhaps resulted as further development of the convective clouds from earlier that day. The green line in Fig. 4b shows that the relative humidity also decreased in the layer between 1 and 5 km, which is also consistent with the lack of convective clouds. The relative vorticity stayed virtually the same, but the vorticity tendency was negative in the lowest level (green lines in Fig. 3a and c, respectively). The saturated moist entropy profile indicates warming at almost all levels (Fig. 4a), green line). The vorticity axis maintained a SW tilt.

On 11 September the third research flight into Karl occurred, with bursts of strong convection to the east of the circulation center. The blue lines in Figs. 3 and 4 refer to Karl 3. The low-level vorticity decreased, but the mid-level vorticity increased so that now the vertical gradient of the area averaged relative vorticity was steeper. The large positive values of the vorticity tendency indicate increasing mid-level vorticity. The vertical mass flux was top-heavy and strong, with a peak near 10 km. At this point Karl became an area of interest to the NHC. The trend of decreasing low-level vorticity and increasing mid-level vorticity continued during the following day. As the Karl 4 research flight did not cover the disturbance adequately on 12 September, this stage of Karl is not documented here. However, NASA's DC8 research aircraft conducted a research flight later that day, and based on the observations NHC reported that "... a surface low pressure system no longer existed beneath a well-defined mid-level circulation".

ACPD
13, 18905–18950, 2013

The sharp increase in the mid-level vorticity was probably a consequence of the strong mass flux gradient in mid-levels during Karl 3. On 13 September the G-V conducted the fifth mission into the disturbance which at that time was located over the warm waters of the northwestern Caribbean Sea. At this point Karl had redeveloped the low-level vortex (purple lines in Figs. 3 and 4). The relative humidity had increased in the lowest 3 km. The saturated moist entropy had decreased in the lower levels and further increased in the upper levels, for a more stable thermodynamic stratification. Convection covered a large fractional area of the observational region. Deep convective and stratiform clouds were observed. The vertical mass flux profile was bottom heavy, reflecting dominance of convective clouds. The relative vorticity was strong in middle levels, corresponding to a cold core vortex. The vortex axis was vertical at that time (not shown) and the largest positive vorticity tendency occurred at low levels. The last mission into Karl was conducted the following day, when the dropsondes registered an earth-relative wind speed of 18 $\mathrm{m\,s^{-1}}$ near the surface. The black lines in Figs. 3 and 4 show the results from this research flight. The relative vorticity had increased at all levels, especially near the surface, and the saturated moist entropy in the upper levels had further increased as well, reflecting even more stable tropospheric stratification.

Karl kept intensifying; on 16 September it reached hurricane strength, and one day later it became a major hurricane. It made a landfall on the Yucatan peninsula, Mexico, and caused significant damage.

In summary, Karl started as a weak vortex in a sheared but moist environment. On the second day (11 September) the vorticity had not changed much, but it featured bursts of deep convection with a top-heavy vertical mass flux profile. This was followed by drastic increase in the mid-level vorticity. Less then 48 h after that, Karl became a tropical storm. The saturated moist entropy in the upper levels featured constant increase from mission to mission, corresponding to stabilization of the troposphere.

ACPD
13, 18905–18950, 2013

S. Gjorgjievska and D. J. Raymond

4.2 Correlation between dynamics and thermodynamics

It has long been known that both dynamics and thermodynamics are involved in the process of tropical storm formation. Dynamics can affect the thermodynamic processes and vice versa, so there is feedback between the two. Hence, in order to understand tropical cyclogenesis one should not only understand both the dynamics and thermodynamics, but should also understand how they work together and how they interact constructively to create a tropical storm. For the purpose of shedding some light on these interactions we investigate possible correlations between different variables that are calculated from observations. The scatter plots presented in this section consist of data points from 31 cases: 24 from PREDICT and 7 from TCS08. All but two cases observed during PREDICT are included in the scatter plots. The test run from PREDICT does not enter because the dropsonde pattern did not enclose any area, and the third mission in Fiona is not considered, as its circulation was strongly influenced by hurricane Earl. Cases like Karl 4, where inadequate area coverage was obtained, are included in the scatter plots. Even though the observational area is not representative of the evolution stage of those cases, we think it is representative of the interactions between dynamics and thermodynamics on the mesoscale. Therefore, we include such cases in the scatter plots. Each data point represents a single mission into a disturbance of interest.

Our analyses showed that the genesis of tropical storm Karl was preceded by development of a mid-level vortex. Two other storms that were observed during PREDICT, Matthew and Nicole, also developed mid-level vortices 24 to 48 h prior genesis (not shown). Only then did the warm-core vortices form. Thus, our results provide more evidence for the top-down pathway of tropical cyclogenesis.

Three scatter plots are shown in Fig. 5. Figure 5a plots the instability index versus the mid-level relative vorticity. The mid-level vorticity is calculated as an area average at 5 km elevation. There is nothing special about this level. We simply choose it as a representative of the mid-level vorticity in all the disturbances, regardless of where the

ACPD
13, 18905–18950, 2013

maximum vorticity occurs in each separate case. The trend in the scatter plot suggests that smaller instability index corresponds to stronger mid-level vorticity. This result is not surprising because it is in agreement with thermal wind balance: mid-level vorticity is associated with cooler lower levels and/or warmer upper levels, which translates into stabilization of the atmosphere, i.e., a decrease of the instability index.

Figure 5b is a scatter plot of instability index versus saturation fraction. It demonstrates negative correlation between these two variables. This says that a more stable troposphere tends to be moister. Figure 5c shows a scatter plot between the instability index and the low-level vorticity tendency. The latter is calculated as an average over the lowest kilometer. The negative slope is obvious, which suggests that larger vorticity tendencies are associated with a more stable troposphere. Figure 5b, c suggests that the thermodynamics associated with strong mid-level vorticity are conducive to the further moistening of the troposphere and to the increase of the near-surface vorticity.

All the scatter plots from Fig. 5 were recreated by calculating the mid-level vorticity as an average between 3 and 5 km, and the low-level vorticity tendency as an average between 0 and 2 km. The trends were very similar to the ones presented here. Moreover, the analagous scatter plots from the other set of results, where minimal area selection was done, imply even stronger correlation between these variables. Therefore, we think the observed trends in the scatter plots are robust.

We do not expect strict correlations between the analyzed variables. It is not even clear if the possible correlations that are implied in the scatter plots are linear or not. The conclusions of our analysis are based solely on the trends that are obvious in the presented scatter plots, positive or negative. Keeping this in mind, one might wonder how strong these correlations might be. Just for a reference, assuming linear correlations between all the variables, we conducted statistical analysis on these data. The correlation coefficients and the p values are given in Table 2. The significance level is greater then 95 % for all the correlations.

ACPD
13, 18905–18950, 2013

S. Gjorgjievska and D. J. Raymond

Title Page
Abstract | Introduction
Conclusions | References
Tables | Figures
◂ | ▸
Back | Close
Full Screen / Esc
Printer-friendly Version
Interactive Discussion

5 Discussion

This paper uses observations from two field programs to explore tropical storm formation. Detailed analyses of two disturbances, one developer and one non-developer that were observed during PREDICT, are documented in Sect. 4.1. The vertical profiles of the various variables presented there represent areal averages. Because of airspace restrictions some of the observational domains were not centered over the target disturbance. Thus, the vertical profiles in Sect. 4.1 most likely differ from what they would be if averaged over the exact area that the respective disturbances cover. Given the small time scales and horizontal scales of convection versus the larger time scales and horizontal scales of mesoscale vorticity, the vertical vorticity profile is probably much less altered then the mass flux profile and it is more robust in representing the big picture of the disturbance behavior, unless the circulation center is entirely outside of the observational domain. Missions where the latter was the case do not enter the analyses in Sect. 4.1. Davis and Ahijevych (2012) have used other data sources in addition to the dropsonde data and have made a different treatment in calculating the vertical circulation profiles of their analyses of Gaston, Karl and Matthew, and the results they obtained do not differ qualitatively from the results presented in this paper.

5.1 The developer versus the decayer/non-redeveloper

In terms of thermodynamics, we saw that in the decaying case (Gaston) the troposphere was moving from more stable towards a more unstable stratification that was reflected in the increase of the saturated moist entropy in the lower levels and decrease in the upper levels. The mid-level vorticity decreased drastically between the first two missions after which vorticity started to decrease continuously at all levels. Time series from the instability index, low-level, and mid-level vorticity for Gaston are given in the left column of Fig. 6. Analogous time series for Karl, the developer, are given in the right column of the same figure. The instability index started low, but it increased between the first two missions into Karl. During that time, the mid-level vortex was

ACPD
13, 18905–18950, 2013

not well developed and it was weaker then the low-level vortex. By the third mission the low-level vorticity had decreased, while the mid-level vortex had intensified. The instability index had further increased, and Karl 3 exhibited a strong, top-heavy mass flux profile (Fig. 3b, blue line). These observed features, i. e. the large instability index in association with the strong top-heavy mass flux profile are in agreement with the theoretical results of Raymond and Sessions (2007); they were looking at the effects of the thermodynamic tropospheric stratification on the vertical convective mass flux profiles. Smith and Montgomery (2012) and Montgomery and Smith (2012) raised concerns about the validity of this study, because it was conducted using a non-rotating cumulus ensemble model. Introducing rotation would probably change the results significantly only if the time scales of convection and vorticity were comparable. Here, we are looking at pre-storm disturbances, where the time scale for vorticity is several times larger then the time scale for convection. Therefore, we believe that introducing rotation would not change the results enough to affect the conclusions of the current work, even though conducting such an experiment might be helpful.

After Karl 3, the troposphere started stabilizing again, as the mid-level vortex strengthened. A day later NHC reported a well developed mid-level circulation and no surface low pressure system beneath it (the cold-core had developed). There are no data from that day in Fig. 6d, but the plot shows almost doubled mid-level relative vorticity from Karl 3 to Karl 5. By the next day Karl had undergone genesis. It appears that the events during Karl 3 were vital for the mid-level vortex development. We discuss this in detail in the next section.

These results emphasize the importance of the mid-level vorticity. Establishment of a mid-level vortex preceded the development of tropical storm Karl. Matthew and Nicole are not documented in this paper, but their genesis was also preceded by a cold-core development with a mid-level vortex. Furthermore, this was observed to be the case with typhoon Robyn (1993) (Harr and Elsberry, 1996) and typhoon Nuri (2008) (Raymond and Lopez, 2011) in the west Pacific, hurricane Guillermo (1991) in the east Pacific (Bister and Emanuel, 1997). There is also evidence of the pre-hurricane

ACPD
13, 18905–18950, 2013

Dolly (1996) in the Atlantic, developing mid-level vortex 35 h before it was upgraded to a TD (Reasor et al., 2005). Two questions naturally follow. The first is what is the mechanism by which the mid-level circulation encourages intensification of the low-level vortex? The second question is why Gaston did not develop, even though it had a mid-level vortex during the first observation? In an effort to gain some understanding of the mechanism addressed in the first question, we looked at scatter plots between various dynamic and thermodynamic variables in Sect. 4.2. We cannot infer causality from these correlations, but we do use the general trends that they reveal between the analyzed variables to propose a mechanism of tropical storm formation. We discuss this mechanism in the next section, and also address the mystery of Gaston there.

5.2 Proposed theory

A low-level mesoscale vortex may or may not exist prior development of a mesoscale mid-level vortex. However, establishment of a mesoscale mid-level vortex occurrs prior to the development/intensification of a low-level cyclonic vortex into a TS. The proposed theory in this paper offers an explanation how the mid-level vortex communicates with the low-level vortex. The Haynes and McIntyre (1987) flux-form of the the vertical vorticity equation does not recognize such communication, as it considers only the dynamics.

We propose that the mid-level vortex promotes development or intensification of the low-level vortex via thermodynamics. Here we compare the tropospheric thermodynamic stratification in a developing and a non-developing case. For a developer we take Karl 5, as genesis occurred less then 48 h later, and for a non-developer we take Gaston 5, as it was an area of interest that never developed. The vertical entropy profiles of both Gaston 5 and Karl 5 are shown in Fig. 7a. The saturated moist entropy indicates that during Karl 5 the lower levels were cooler in comparison to Gaston 5, and the upper levels were warmer. This is in agreement with thermal wind balance, since unlike Gaston 5, Karl 5 featured a well-developed mid-level vortex. That vortex is expected to be associated with cooler lower levels and warmer upper levels.

ACPD
13, 18905–18950, 2013

S. Gjorgjievska and D. J. Raymond

The result is that in the developing case the troposphere is more stably stratified, as Fig. 7a shows. How does this new stratification affect the dynamics? It forces the dynamics indirectly, by forcing a different type of convection. When the troposphere is more stably stratified, the convection produces a more bottom-heavy mass flux profile. Comparison between the mass fluxes is given in Fig. 7b. In the developing case we see bottom-heavy vertical mass flux, with a large positive gradient in the lowest 3 km. Thinking in terms of mass continuity, the largest horizontal convergence occurs at levels where the vertical gradient of the vertical mass flux is the largest. This is demonstrated in Fig. 7c, which represents vertical profiles of the horizontal mass divergence. More negative values represent stronger convergence. Thus, in case of Karl 5 the near surface convergence is more then double that in Gaston 5. The opposite is true for the mid-levels. Thus, in the development of the low-level cyclone, the convergence is strong at low levels, where the moist entropy has large values. At mid-levels on the other hand, where moist entropy exhibits a minimum, convergence is small to non-existent. This situation ultimately results in moist entropy increase within the disturbance. For the non-developer the convergence in the mid-levels is comparable to that at low levels, so the moistening at the low levels is overcompensated by drying at mid-levels. Thus, there are two consequences of the low-level mass convergence that are important for tropical storm formation. One is low-level vorticity convergence, which leads to immediate low-level vortex intensification. The other consequence is the stronger moist entropy convergence, which supports humidification of the column and further moist convection.

In summary, based on the analysis presented in this paper, we propose the following chain of events for tropical cyclogenesis: Dynamics and thermodynamics are equally important and have complementary roles in the process of tropical storm formation. The necessary ingredient is a well-developed mid-level vortex that by the virtue of thermal wind balance maintains a more stable atmosphere. We saw from observations that indeed stronger mid-level vorticity was associated with a lower instability index (Fig. 5a). The more stable atmosphere is conducive to moist convection that produces

ACPD
13, 18905–18950, 2013

a mass flux profile with the largest positive vertical gradient in a shallow layer adjacent to the sea surface. Mass continuity then dictates horizontal mass convergence at low levels, where most of the water vapor is contained. Mass convergence near the surface means water vapor convergence and low-level vorticity convergence. Hence the negative correlations between the instability index and the saturation fraction (Fig. 5b) and between the instability index and the low-level vorticity tendency (Fig. 5c). If the mid-level vorticity exists long enough to keep this chain of events going, the low-level wind speed will eventually reach the tropical storm threshold.

In relation to the "bottom-up" development hypothesis, the theory we present here does not contradict the importance of a protected pouch where convection occurs uninterrupted. It also does not dispute the idea that the low-level vortex intensifies as a result of aggregation of vorticity produced by deep convection. According to our theory, though, the type of this convection is such that it produces vertical convective mass fluxes with the strongest positive vertical gradient in a shallow layer near the surface. The mid-level vortex is necessary to maintain thermodynamic stratification on the mesoscale that is conducive for such convection.

5.3 The mystery of Gaston

Tropical storm Gaston presented a real mystery, as it decayed in the face of strong expectations that it would intensify. Davis and Ahijevych (2012) and Smith and Montgomery (2012) hypothesized that Gaston decayed as a result of dry air intrusion. The presence of dry air surrounding Gaston was indeed evident on satellite images. However, we are skeptical of the role of dry air in the *initial* decay, as the vertical profile of relative humidity was virtually the same during the first two observations of Gaston (see Fig. 2b). Figure 8a, b shows high saturation fraction, with a maximum near the 5 km circulation center, for both Gaston 1 and Gaston 2. We also looked at the longitude-latitude distribution of the relative humidity and the relative wind at multiple levels on these two consecutive days, and did not find evidence of dry air intrusion (Fig. 9 shows the 5 and 7 km levels). Nor did the Lagrangian analysis of Rutherford and Montgomery

ACPD
13, 18905–18950, 2013

(2012) show dry air intrusion between the first two Gaston missions. It appears that the closed circulation of Gaston 1 at both low and middle levels prevented dry air intrusion into the core at this point of Gaston's evolution. We do not question the existence of dry air intrusion after Gaston 2. As the above cited papers showed, and as is reflected in our Fig. 9b, the drying of the disturbance started after the second mission into this disturbance.

We attribute Gaston's ultimate decay to the dissipation of its initially observed mid-level vortex between Gaston 1 and Gaston 2 (see Fig. 1a). Here we explore possible factors that caused this dissipation. We also compare Gaston 1 and Karl 3, as we find that events observed in these two missions were critical to the subsequent success or failure of the respective systems, and the contrast between the two is instructive.

The decrease in the mid-level vorticity from Gaston 1 to Gaston 2 we find to be due to the form of the vertical mass flux profile observed during Gaston 1. The left panels in Fig. 10 show the vertical mass flux at 3 km and at 6 km elevation for Gaston 1. Positive vertical mass flux existed near the circulation center in Gaston. However, it was weak in the upper levels and it covered a small area. The right panels in Fig. 10 show analogous plots for Karl 3. Convection in Karl 3 was stronger at higher levels and it covered a much larger area compared to that of Gaston 1. The black boxes in this figure enclose most of the convective activity.

Vertical mass flux profiles for both Gaston 1 and Karl 3, horizontally averaged over the respective black boxes in Fig. 10, are shown in Fig. 11. Consistent with the high instability index previously calculated, Karl 3 had a top-heavy mass flux profile with a maximum vertical mass flux at 10 km. In response to this, Karl exhibited strong mass and vorticity convergence at middle levels and therefore intensified mid-level vorticity between Karl 3 and Karl 5. Gaston 1 on the other hand, consistent with the low instability index, had a bottom-heavy vertical mass flux profile. It exhibited a maximum at about 3 km, and decreased sharply above that level. The positive vertical gradient of the mass flux in the lowest 3 km implies mass and vorticity convergence at low levels. As a result, the low-level vortex intensified from Gaston 1 to Gaston 2. However, the

ACPD
13, 18905–18950, 2013

negative vertical gradient of the mass flux above 3 km implies mass divergence at middle levels, and thus vorticity divergence. It seems likely that the decrease in mid-level relative vorticity in this interval weakened the protective pouch at middle levels and allowed dry air intrusion. The dry air sealed the fate of Gaston, as described by Davis and Ahijevych (2012), Smith and Montgomery (2012), and Rutherford and Montgomery (2012). In summary, this entire sequence of events appeared to follow from the weak, bottom-heavy mass flux profile during Gaston 1.

Why was the Gaston 1 mass flux profile so different from that of Karl 3? There are three possibilities for this. First, dry air might have been drawn into the core of Gaston; second, weaker surface fluxes may have affected Gaston 1, due to lower SSTs; and third, buoyancy adjustment from the surroundings tended to stabilize the column in Gaston. The first possibility is unlikely, as discussed above, due to the robust pouch in Gaston 1. Now we explore the other two possibilities.

Figure 12a shows the Reynolds SST for Gaston 1. The overlying vector field is the system-relative wind averaged between 0 and 1 km. The SST below the circulation center is $\sim 28.5\,^{\circ}$C and it decreases northward. Though these SSTs are above the threshold for tropical storm development, they are $2\,^{\circ}$C cooler then the corresponding SSTs for Karl 3 (Fig. 12b). This difference in SSTs is potentially important for the difference in the mass flux profiles.

Now we explore moist entropy and buoyancy of ascending surface parcels in Gaston 1 and Karl 3 (see Appendix for buoyancy calculation). We calculated these variables as averages over dropsondes from the respective disturbance, within the area selected for analysis. We averaged separately over the dropsondes within the respective black boxes (see Fig. 12) that enclose most of the convectively active regions, and over the dropsondes outside these regions, but still within the selected area for analysis. The results are shown in Fig. 13.

The vertical profile of the saturated moist entropy for Gaston 1 (red line in Fig. 2a) indicates temperature inversion layer between 1 and 2 km. This inversion is most likely related to the underlying low SST. Figure 13a, b shows that this inversion exists primer-

ACPD
13, 18905–18950, 2013

ily outside the black box. Within the convectively active region the buoyancy profile does not show evidence of an inversion (Fig. 13b), most likely because convection locally destroys the inversion. Outside the black box in Gaston 1 both saturated moist entropy and buoyancy indicate a strong trade wind inversion and overall much smaller magnitude of buoyancy. In contrast, the corresponding entropy and buoyancy vertical profiles of Karl 3 (Fig. 13c, d) show no evidence of an inversion inside or outside of the convectively active region, which is consistent with the high values of the underlying SSTs. There is a notable difference between the buoyancy profiles of Gaston 1 and Karl 3. For Gaston 1 there is a big difference in buoyancy within and outside the convectively active region, whereas for Karl 3, this difference is much smaller. Thus, the larger environment (outside the box) for Karl 3 is conducive to convection, and for Gaston 1 it is very unfavorable. We hypothesize that in Gaston 1 convection is modifying buoyancy locally, and thus the inversion is reduced in the region of convective activity, while at the same time the trade wind dynamics is reinforcing the temperature inversion, which further suppresses convection.

In summary, our analyses demonstrate a hostile environment for convection in Gaston 1 in the form of a strong trade wind inversion. We hypothesize that this inversion, originating from the relatively low SSTs, was the most important factor in the sharp decrease of the mid-level vorticity from Gaston 1 to Gaston 2. Low relative humidity above 6 km may have been an additional factor, but this effect was likely weak due to the low saturation mixing ratio and hence low saturation deficit at high elevations. Dry air surrounded Gaston at middle levels, but appeared to be unable to penetrate to the core due to the protective pouch produced by the mid-level vortex, thus limiting its direct effect on convection during Gaston 1.

As expected from our theory, the low instability index of Gaston 1 resulted in a bottom-heavy convective mass flux profile. This profile caused the observed intensification of the low-level vortex between Gaston 1 and Gaston 2. However, the negative gradient of the mass flux profile above the maximum, due most likely to the strong trade wind inversion, caused the mid-level vortex to weaken significantly during the same pe-

ACPD
13, 18905–18950, 2013

Interaction between dynamics and thermodynamics

S. Gjorgjievska and D. J. Raymond

riod. This led to the collapse of the pouch at mid-levels and the subsequent intrusion of dry air into Gaston's core, resulting in its failure to develop.

6 Conclusions

In this paper we analyzed data from tropical disturbances that were observed during PREDICT and TCS08, focusing on the evolution of two systems. One (Karl) developed into a major hurricane and the other (Gaston) decayed after briefly becoming a minimal tropical storm. We found that the development of a strong mid-level vortex preceded low-level vortex intensification in the developer, and divergence of mid-level vorticity preceded weakening of the low-level vortex in the decayer. This paper researched the influence of the mid-level vorticity on the low-level vortex. We created scatter plots between various dynamic and thermodynamic variables in order to understand the mechanism by which the mid-level vortex leads to low-level spin up. Based on the trends that we found in the scatter plots and on previous work by Raymond and Sessions (2007), we propose a hybrid hypothesis that explains the communication between the mid- and low-level vortices. The mid-level vortex is associated via balanced dynamics with cooler lower levels and warmer upper levels. This more stable thermodynamic stratification is conducive to moist convection that produces vertical mass flux profiles with the largest positive vertical gradient in the lowest few kilometers. By virtue of mass continuity, this means that the strongest horizontal mass convergence occurs near the surface. This implies positive vorticity tendency near the surface and low-level vortex spin up.

Karl was a disturbance that closely followed our theory. It was observed in the 4 day period before it become a tropical storm. It started with a low-level cyclonic vortex and a weaker mid-level vortex, but it did not start intensifying until it developed a strong mid-level vortex. The development of the mid-level vortex followed as a result of the strong, top-heavy vertical mass flux profile that was observed during Karl 3. This profile is consistent with the high instability index that existed at that time. Karl 5 exhibited strong

Discussion Paper | Discussion Paper | Discussion Paper | Discussion Paper |

ACPD
13, 18905–18950, 2013

Interaction between dynamics and thermodynamics

S. Gjorgjievska and D. J. Raymond

mid-level vorticity and low instability index which resulted in low-level vortex spin up between Karl 5 and Karl 6.

Gaston was first observed only a couple of hours after it decayed from a tropical storm to a tropical depression. During this first observation Gaston still had a strong mid-level vortex, which weakened significantly until the second mission into this disturbance. We believe that this was the crucial element in Gaston's decay. We further hypothesize that convection was suppressed by a strong trade wind inversion. Convection at the time of the observation was concentrated in a small area near the 5 km circulation center. It produced bottom-heavy vertical profile of the convective mass flux that decreased with altitude in the middle troposphere. Though the bottom-heavy mass flux profile produced a transient intensification of the low-level vortex, the negative vertical gradient of the mass flux above 3 km was responsible for the negative vorticity tendency in the middle levels and therefore the decrease in mid-level vorticity by the following day. The divergence of the mid-level vorticity exposed Gaston to the ingestion of dry environmental air, which sealed its fate.

Appendix

Buoyancy calculation

We calculate the buoyancy as follows:

$$b = -g(T_v - T_{vp})/T_v. \tag{A1}$$

T_v is the environmental virtual temperature,

$$T_v = T(1 + 0.00061r), \tag{A2}$$

and T_{vp} is the parcel virtual temperature,

$$T_{vp} = T_p(1 + 0.00061r_p). \tag{A3}$$

Discussion Paper | Discussion Paper | Discussion Paper | Discussion Paper |

ACPD

13, 18905–18950, 2013

Interaction between dynamics and thermodynamics

S. Gjorgjievska and D. J. Raymond

T_p is the parcel temperature at each level and it is calculated as the environmental temperature plus a temperature perturbation, δT, of the parcel at each level. The latter is estimated by using the approximate formulas (7) and (8) from RSL11:

$$\delta T = \delta s^*/(\partial s^*/\partial T)_p \approx \delta s^*/(3.7 + 0.64 r^*), \tag{A4}$$

where we calculate δs^* as:

$$\delta s^* = s^* - s_0. \tag{A5}$$

Here s_0 is the specific moist entropy averaged over the lowest kilometer and s^* is the saturated moist entropy of the environment. The variable $r_p = r_p(z)$ in Eq. (A3) is the mixing ratio of the parcel, which we calculate from the pressure and T_p, under assumption that the parcel is saturated. We use the formula:

$$r_p = 0.622 \frac{e_s(T_p)}{p - e_s(T_p)}, \tag{A6}$$

where e_s is the saturation vapor pressure calculated from the Clausius–Clapyron equation.

Supplementary material related to this article is available online at: http://www.atmos-chem-phys-discuss.net/13/18905/2013/acpd-13-18905-2013-supplement.pdf.

Acknowledgements. We thank the dedicated staff of the NSF/NCAR G-V operation for their excellent work. Data provided by NCAR/EOL under sponsorship of the National Science Foundation. This work was supported by National Science Foundation grants 0851663 and 1021049, and the Office of Naval Research grant N000140810241.

ACPD
13, 18905–18950, 2013

References

Bister, M. and Emanuel, K. A.: The genesis of hurricane Guillermo: TEXMEX analyses and a modeling study, Mon. Weather Rev., 125, 2662–2682, 1997. 18908, 18922

Bretherton, C. S., Peters, M. E., and Back, L. E.: Relationships between water vapor path and precipitation over the tropical oceans, J. Climate, 17, 1517–1528, 2004.

Bryan, G. H. and Rotunno, R.: The maximum intensity of tropical cyclones in axisymmetric numerical model simulations, Mon. Weather Rev., 137, 1770–1789, 2009.

Charney, J. G. and Eliassen, A: On the growth of the hurricane depression, J. Atmos. Sci., 21, 68–75, 1963.

Davidson, N. E., Holland, G. J., McBride, J. L., and Keenan, T. D.: On the formation of AMEX tropical cyclones Irma and Jason, Mon. Weather Rev., 118, 1981–2000, 1990.

Davis, C. A. and Ahijevych, D. A.: Mesoscale structural evolution of three tropical weather systems observed during PREDICT, J. Atmos. Sci., 69, 1284–1305, 2012. 18908, 18925, 18927

Dunkerton, T. J., Montgomery, M. T., and Wang, Z.: Tropical cyclogenesis in a tropical wave critical layer: easterly waves, Atmos. Chem. Phys., 9, 5587–5646, doi:10.5194/acp-9-5587-2009, 2009. 18907

Emanuel, K. A.: An air–sea interaction theory for tropical cyclones, Part 1: Steady-state maintenance, J. Atmos. Sci., 43, 585–604, 1986.

Elsberry, R. L. and Harr, P. A.: Tropical cyclone structure (TCS08) field experiment science basis, observational platforms, and strategy, Asia-Pacific J. Atmos. Sci., 44, 209–231, 2008.

Gray, W. M.: Global view of the origin of tropical disturbances and storms, Mon. Weather Rev., 96, 3380–3403, 1968. 18906

Gray, W. M.: Environmental influences on tropical cyclones, Aust. Met. Mag., 36, 127–139, 1988.

Haynes, P. and McIntyre, M.: On the evolution of vorticity and potential vorticity in the presence of diabatic heating and fractional or other forces, J. Atmos. Sci., 44, 828–841, 1987. 18923

Harr, P. A. and Elsberry, R. L.: Transformation of a large monsoon depression to a tropical storm during TCM-93, Mon. Weather Rev., 124, 2625–2643, 1996. 18908, 18922

Houze Jr., R. A., Lee, W. C., and Bell, M. M.: Convective contribution to the genesis of hurricane Ophelia (2005), Mon. Weather Rev., 137, 2778–2800, 2009.

Kurihara, Y.: Budget analysis of a tropical cyclone simulated in an axisymmetric numerical model, J. Atmos. Sci., 32, 25–59, 1975.

ACPD
13, 18905–18950, 2013

Interaction between dynamics and thermodynamics

S. Gjorgjievska and D. J. Raymond

Title Page
Abstract | Introduction
Conclusions | References
Tables | Figures
◀ | ▶
Back | Close
Full Screen / Esc
Printer-friendly Version
Interactive Discussion

López Carrillo, C. and Raymond, D. J.: Retrieval of three-dimensional wind fields from Doppler radar data using an efficient two-step approach, Atmos. Meas. Tech., 4, 2717–2733, doi:10.5194/amt-4-2717-2011, 2011. 18910

Malkus, J. C. and Riehl, H.: On the dynamics and energy transformations in a steady-state hurricane, Tellus, 12, 1–20, 1960.

McBride, J. L. and Zehr, R.: Observational analysis of tropical cyclone formation, Part 2: Comparison of non-developing versus developing systems, J. Atmos. Sci., 38, 1132–1151, 1981. 18907

Molinari, J., Skubis, S., and Vollaro, D.: External influences on hurricane intensity, Part 3: Potential vorticity structure, J. Atmos. Sci., 22, 3593–3606, 1995.

Montgomery, M. T. and Smith, R. K.: The genesis of Typhoon Nuri as observed during the Tropical Cyclone Structure 2008 (TCS08) field experiment – Part 2: Observations of the convective environment, Atmos. Chem. Phys., 12, 4001–4009, doi:10.5194/acp-12-4001-2012, 2012. 18922

Montgomery, M. T., Sang, N. V., Smith, R. K., and Persing, J.: Do tropical cyclones intensify by WISHE?, Q. J. Roy. Meteorol. Soc., 135, 1697–1714, 2009.

Montgomery, M. T., Wang, Z., and Dunkerton, T. J.: Coarse, intermediate and high resolution numerical simulations of the transition of a tropical wave critical layer to a tropical storm, Atmos. Chem. Phys., 10, 10803–10827, doi:10.5194/acp-10-10803-2010, 2010.

Montgomery, M. T., Davis, C., Dunkerton, T., Wang, Z., Velden, C., Torn, R., Majumdar, S. J., Zhang, F., Smith, R. K., Bosart, L., Bell, M. M., Haase, J. S., Heymsfield, A., Jensen, J., Campos, T., and Boothe, M. A.: The Pre-Depression Investigation of Cloud-systems in the Tropics (PREDICT) experiment, B. Am. Meteorol. Soc., 93, 153–172, 2012. 18909

Nolan, D. S.: What is the trigger for tropical cyclogenesys?, Aust. Met. Mag., 56, 241–266, 2007.

Ooyama, K. V.: Numerical simulation of the life cycle of tropical cyclones, J. Atmos. Sci., 26, 3–40, 1969.

Ooyama, K. V.: Conceptual evolution of the theory and modeling of the tropical cyclone, J. Atmos. Sci. Japan, 60, 369–379, 1982.

Raymond, D. J. and Fuchs, Z.: Moisture modes and the Madden–Julian oscillation, J. Climate, 22, 3031–3046, 2009.

Raymond, D. J. and Jiang, H.: A theory for long-lived mesoscale convective systems, J. Atmos. Sci., 47, 3067–3077, 1990.

ACPD
13, 18905–18950, 2013

Raymond, D. J. and López Carrillo, C.: The vorticity budget of developing typhoon Nuri (2008), Atmos. Chem. Phys., 11, 147–163, doi:10.5194/acp-11-147-2011, 2011. 18908, 18909, 18910, 18922

Raymond, D. J. and Sessions, S. L.: Evolution of convection during tropical cyclogenesis, Geophys. Res. Lett., 34, L06811, doi:10.1029/2006GL028607, 2007. 18922, 18929

Raymond, D. J., Lopez Carillo, C., and Lopez Cavazos, L.: Case-studies of developing east Pacific easterly waves, Q. J. Roy. Meteorol. Soc., 124, 2005–2034, 1998. 18908

Raymond, D. J., Sessions, S. L., and Lopez Carrillo, C.: Thermodynamics of tropical cyclogenesis in the Northwest Pacific, J. Geophys. Res., 116, D18101, doi:10.1029/2011JD015624, 2011. 18908

Reasor, P. D., Montgomery, M. T., and Bosart, L. F.: Mesoscale observations of the genesis of Hurricane Dolly (1996), J. Atmos. Sci., 62, 3151–3171, 2005. 18923

Rotunno, R. and Emanuel, K. A.: An air–sea interaction theory for tropical cyclones, Part 2: Evolutionary study using a nonhydrostatic axisymmetric numerical model, J. Atmos. Sci., 44, 542–561, 1987.

Rutherford, B. and Montgomery, M. T.: A Lagrangian analysis of a developing and non-developing disturbance observed during the PREDICT experiment, Atmos. Chem. Phys., 12, 11355–11381, doi:10.5194/acp-12-11355-2012, 2012. 18925, 18927

Smith, R. K. and Montgomery, M. T.: Observations of the convective environment in developing and non-developing tropical disturbances, Q. J. Roy. Meteorol. Soc., 138, 1721–1739, 2012. 18916, 18922, 18925, 18927

Smith, R. K., Montgomery, M. T., and Vogl, S.: A critique of Emanuel's hurricane model and potential intensity theory, Q. J. Roy. Meteorol. Soc., 134, 551–561, 2008.

Wang, Z., Montgomery, M. T., and Dunkerton, T. J.: Genesis of pre-Hurricane Felix (2007), Part 1: The role of the easterly wave critical Layer, J. Atmos. Sci., 67, 1711–1729, 2010.

Wang, Z., Montgomery, M. T., and Dunkerton, T. J.: Genesis of pre-Hurricane Felix (2007), Part 2: Warm core formation, precipitation evolution, and predictability, J. Atmos. Sci., 67, 1730–1744, 2010.

Table 1. Observational cases that enter the scatter plots in Sect. 4.2. The stage of each disturbance is as recognized by NHC at the time of observation. "Low" stands for either a tropical wave or a weak tropical disturbance, while TD indicates a tropical depression and TS a tropical storm.

	date	ref. time	$\boldsymbol{v}_p$ [m s^{-1}]	SST [°C]	stage
PGI27-1	17 Aug 2010	12:00	(−8.0, 0.0)	29.8	low
PGI27-2	18 Aug 2010	14:30	(−7.0, 0.0)	29.6	low
PGI30-1	21 Aug 2010	14:00	(−8.0, 0.0)	28.0	not classified
PGI30-2	23 Aug 2010	12:00	(−7.0, 2.5)	29.4	not classified
Fiona 1	30 Aug 2010	13:00	(−8.9, 0.0)	28.5	low
Fiona 2	31 Aug 2010	13:00	(−10.1, 3.7)	29.3	TD
Gaston 1	2 Sep 2010	17:00	(−3.0, 1.0)	28.2	TD
Gaston 2	3 Sep 2010	16:00	(−3.1, 1.8)	28.4	low
Gaston 3	5 Sep 2010	16:00	(−6.7, 0.0)	28.7	low
Gaston 4	6 Sep 2010	14:00	(−6.7, 0.0)	29.1	low
Gaston 5	7 Sep 2010	14:00	(−6.7, 0.0)	29.4	low
Karl 1	10 Sep 2010	11:15	(−5.1, 0.0)	30.0	not classified
Karl 2	10 Sep 2010	19:00	(−2.0, 0.9)	30.0	not classified
Karl 3	11 Sep 2010	17:45	(−6.0, 0.0)	30.2	low
Karl 4	12 Sep 2010	21:40	(−6.8, 0.0)	30.0	low
Karl 5	13 Sep 2010	13:45	(−6.1, 2.8)	30.1	low
Karl 6	14 Sep 2010	17:00	(−6.1, 2.8)	30.0	TS
Matthew 1	20 Sep 2010	15:00	(−5.1, −1.5)	29.9	low
Matthew 2	21 Sep 2010	14:30	(−6.0, 0.0)	30.1	low
Matthew 3	22 Sep 2010	16:00	(−6.0, 0.0)	29.8	low
Matthew 4	24 Sep 2010	16:00	(−8.9, 0.0)	29.7	TS
Nicole 1	27 Sep 2010	16:00	(0.0, 0.0)	29.6	low
Nicole 2	28 Sep 2010	16:00	(1.5, 4.2)	29.6	TS
PGI48/50	30 Sep 2010	15:15	(−6.2, 2.3)	29.5	low

ACPD
13, 18905–18950, 2013

Table 1. Continued.

	date	ref. time	$\mathbf{v}_p$ [m s^{-1}]	SST [°C]	stage
Nuri 1	15 Aug 2008	25:50	(−7.0, 0.0)	29.8	low
Nuri 2	16 Aug 2008	23:55	(−8.7, 0.0)	29.9	TD
TCS025-1	27 Aug 2008	00:00	(2.4, 2.6)	29.5	low
TCS025-2	28 Aug 2008	00:00	(2.4, 2.6)	29.2	low
TCS030	1 Sep 2008	24:00	(−6.3, 0.6)	30.1	low
TCS037	7 Sep 2008	21:05	(−5.7, 3.2)	28.2	low
Hagupit 2	14 Sep 2008	23:35	(−2.3, 1.1)	29.9	low

ACPD
13, 18905–18950, 2013

S. Gjorgjievska and D. J. Raymond

Table 2. Statistics on the scatter plots in Fig. 5.

variables	correlation coeff.	*p* value
mid-level vorticity vs. instability index	0.32	0.04
instability index vs. saturation fraction	0.60	0.0002
instability index vs. low-level vorticity tendency	0.35	0.05

ACPD
13, 18905–18950, 2013

Interaction between dynamics and thermodynamics

S. Gjorgjievska and D. J. Raymond

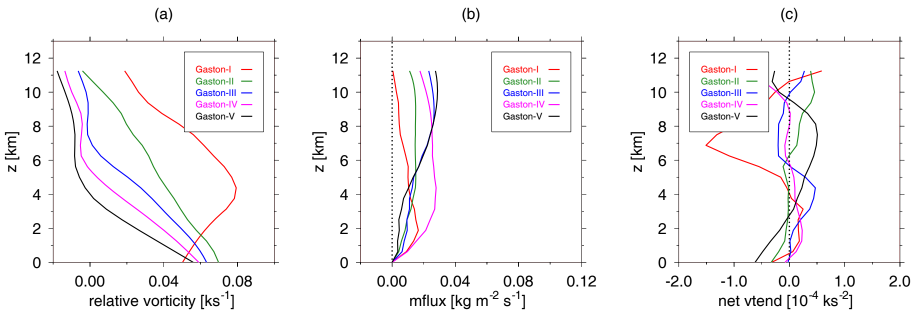

Fig. 1. Horizontally averaged **(a)** relative vertical vorticity, **(b)** vertical mass flux, and **(c)** vorticity tendency for all the Gaston missions.

ACPD
13, 18905–18950, 2013

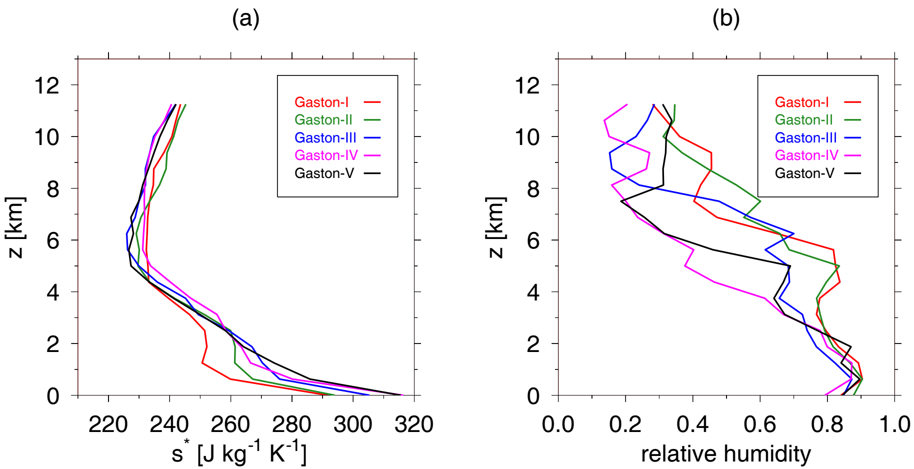

Fig. 2. Horizontally averaged **(a)** saturated moist entropy and **(b)** relative humidity for all the Gaston missions.

Discussion Paper | Discussion Paper | Discussion Paper | Discussion Paper |

ACPD

13, 18905–18950, 2013

Interaction between dynamics and thermodynamics

S. Gjorgjievska and D. J. Raymond

Title Page
Abstract Introduction
Conclusions References
Tables Figures
◀I ▶I
◀ ▶
Back Close
Full Screen / Esc
Printer-friendly Version
Interactive Discussion

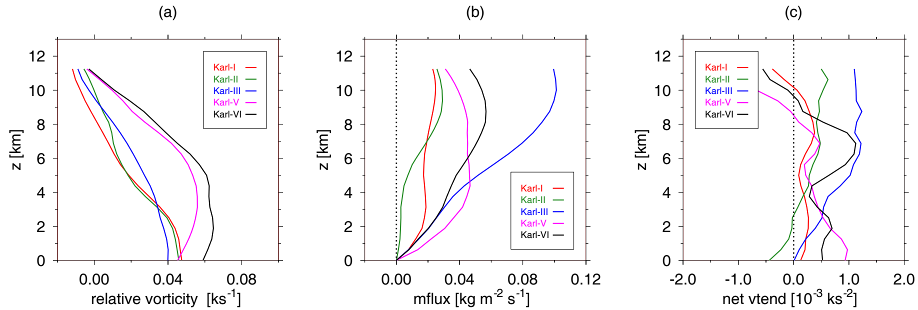

Fig. 3. Same as Fig. 1, but for Karl.

ACPD
13, 18905–18950, 2013

Interaction between dynamics and thermodynamics

S. Gjorgjievska and D. J. Raymond

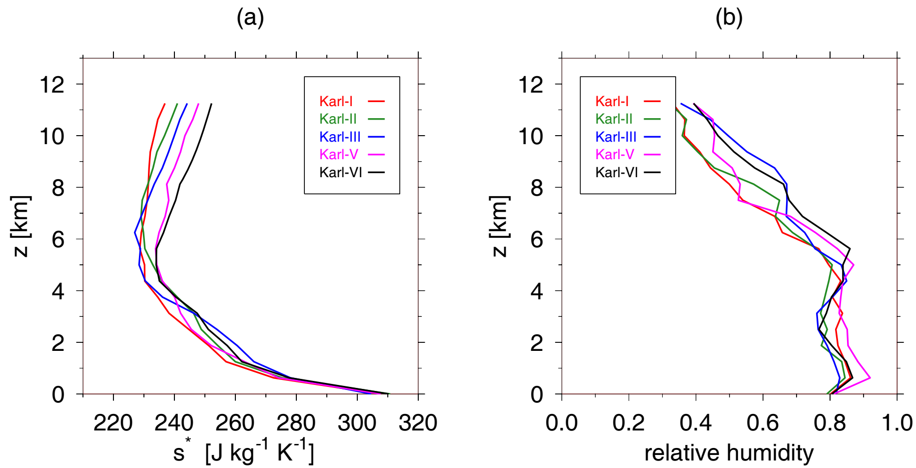

Fig. 4. Same as Fig. 2, but for Karl.

ACPD
13, 18905–18950, 2013

Interaction between dynamics and thermodynamics

S. Gjorgjievska and D. J. Raymond

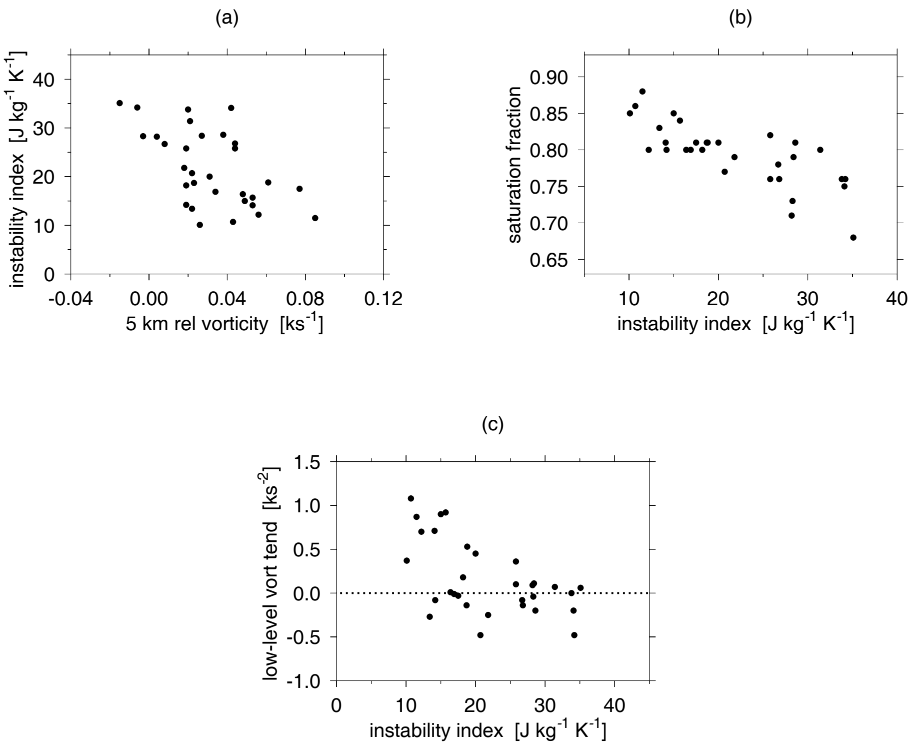

Fig. 5. Scatter plots of **(a)** mid-level relative vorticity versus instability index, **(b)** instability index versus saturation fraction, and **(c)** instability index versus low-level vorticity tendency.

ACPD
13, 18905–18950, 2013

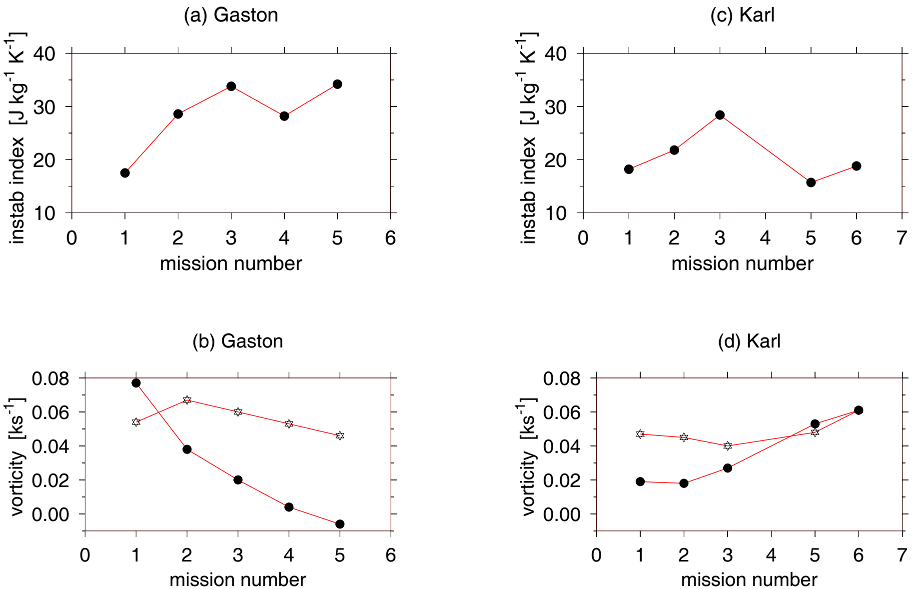

Fig. 6. Gaston **(a, b)** and Karl **(c, d)**. The solid circles in the bottom panels are for the mid-level relative vorticity and the stars are for the low-level relative vorticity.

ACPD
13, 18905–18950, 2013

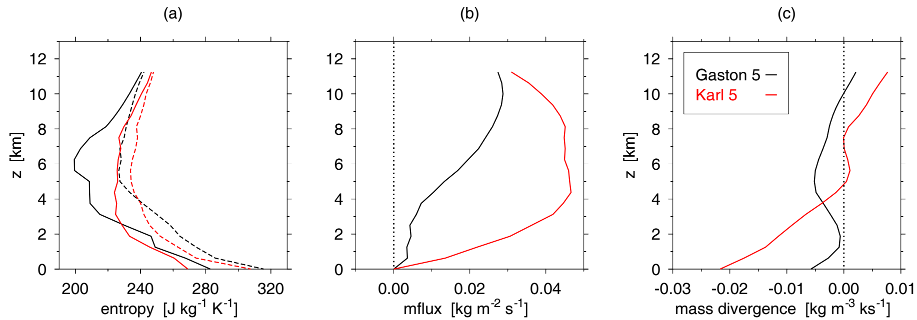

Fig. 7. Vertical profiles of **(a)** moist entropy (solid lines) and saturated moist entropy (dashed lines), **(b)** vertical mass flux, and **(c)** horizontal mass divergence for Gaston 5 and Karl 5.

ACPD
13, 18905–18950, 2013

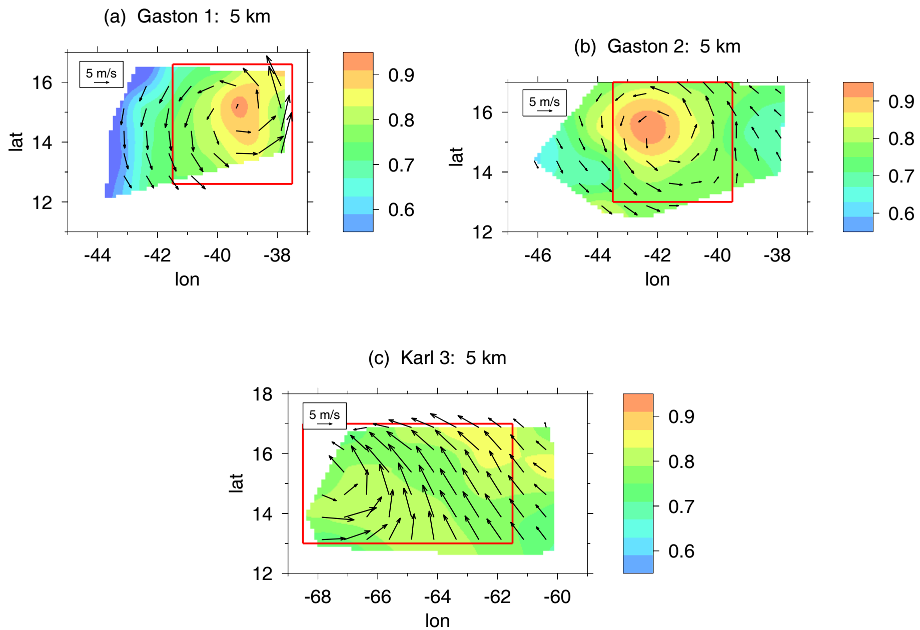

Fig. 8. Saturation fraction and the relative wind at 5 km elevation for **(a)** Gaston 1, **(b)** Gaston 2, and **(c)** Karl 3. The red boxes enclose the area selected for analysis.

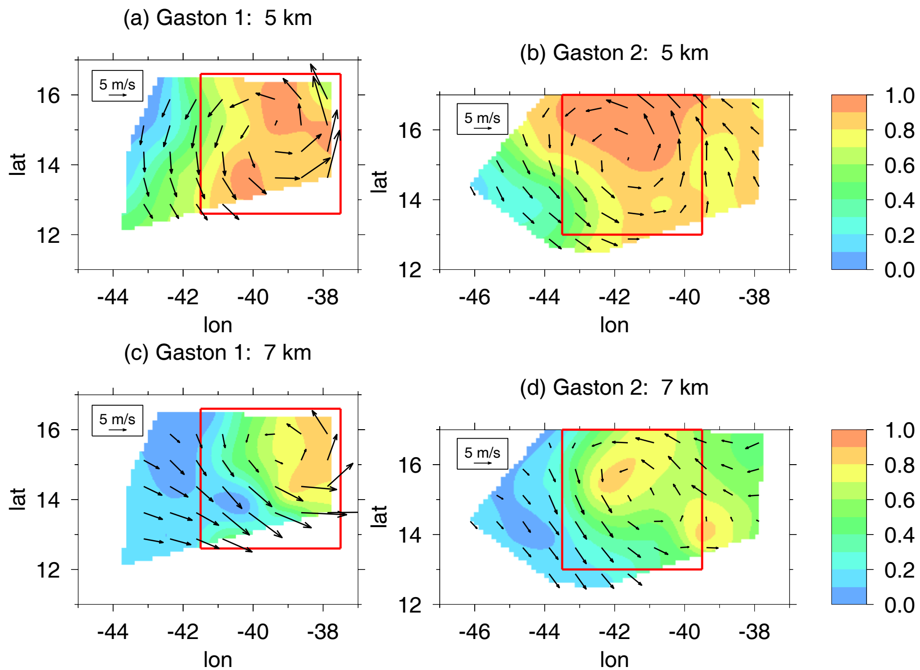

Fig. 9. Relative humidity during Gaston 1 **(a, c)** and Gaston 2 **(b, d)** at 5 km and at 7 km. The vectors represent the relative wind at the respective levels. The red boxes enclose the area selected for analysis.

ACPD
13, 18905–18950, 2013

Interaction between dynamics and thermodynamics

S. Gjorgjievska and D. J. Raymond

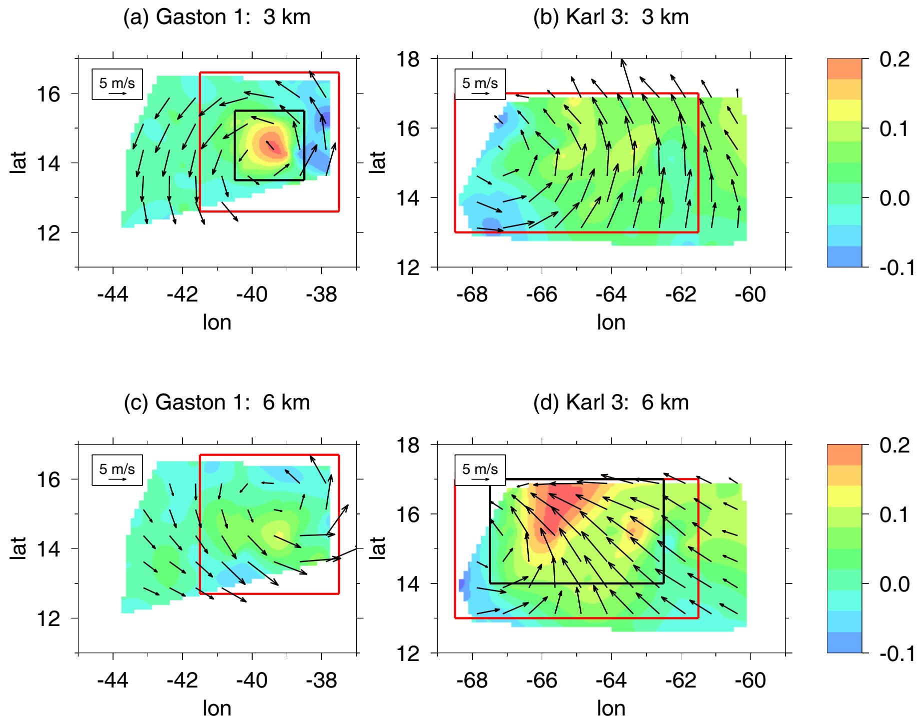

Fig. 10. Vertical mass flux and relative wind at 3 km and at 6 km for Gaston 1 **(a, c)** and Karl 3 **(b, d)**. The units are kg m^{-2}s^{-1}. The red boxes enclose the area selected for analysis, and the black boxes enclose area of convective activity.

ACPD
13, 18905–18950, 2013

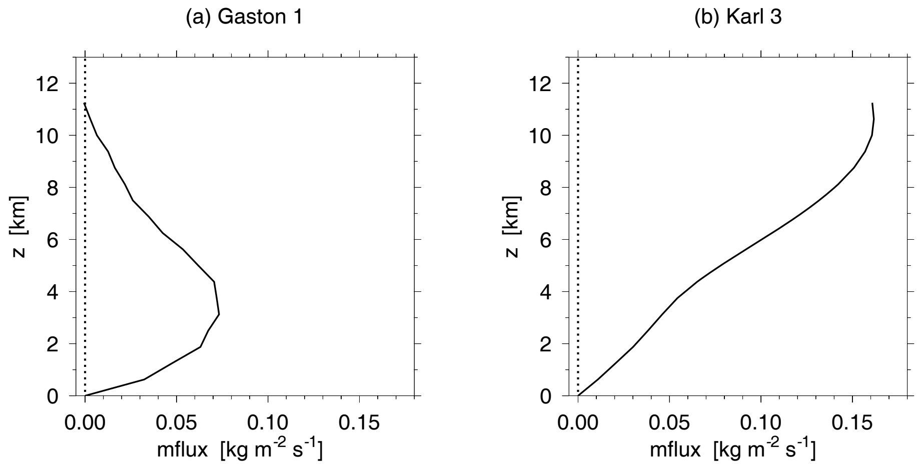

Fig. 11. Vertical mass flux profiles averaged over the black boxes in Fig. 10 for Gaston 1 **(a)** and Karl 3 **(b)**.

ACPD
13, 18905–18950, 2013

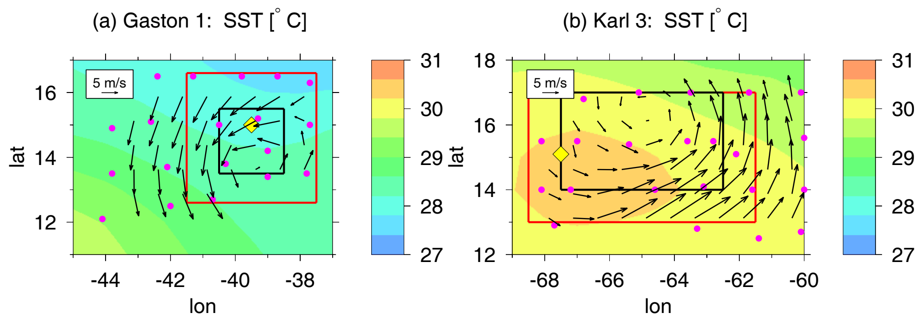

Fig. 12. Reynolds SST (units are °C) for Gaston 1 **(a)** and Karl 3 **(b)**. The vectors represent the relative wind, averaged over the lowest kilometer. The purple dots indicate dropsonde positions, and the yellow diamond marks the circulation center at 5 km.

ACPD
13, 18905–18950, 2013

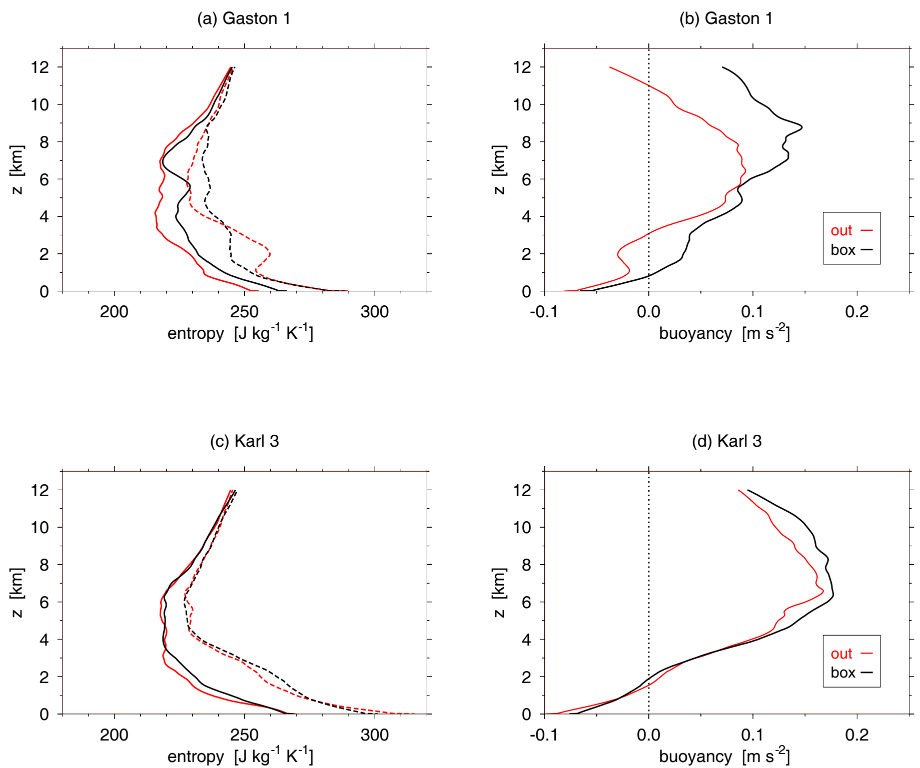

Fig. 13. Vertical profiles of **(a)** moist entropy (solid lines) and saturated moist entropy (dashed lines) for Gaston 1, **(b)** buoyancy for Gaston 1, **(c)** moist entropy (solid lines) and saturated moist entropy (dashed lines) for Karl 3, and **(d)** buoyancy for Karl 3. The black lines represent averages over the dropsondes outside the respective red box in Fig. 12, and the red lines represent averages over the dropsondes enclosed with the respective red box in Fig. 12.

ACPD
13, 18905–18950, 2013

S. Gjorgjievska and D. J. Raymond